

IEEE JOURNAL OF SELECTED TOPICS IN APPLIED EARTH OBSERVATIONS AND REMOTE SENSING

A PUBLICATION OF THE IEEE GEOSCIENCE AND REMOTE SENSING SOCIETY
AND THE IEEE COMMITTEE ON EARTH OBSERVATIONS



MARCH 2016

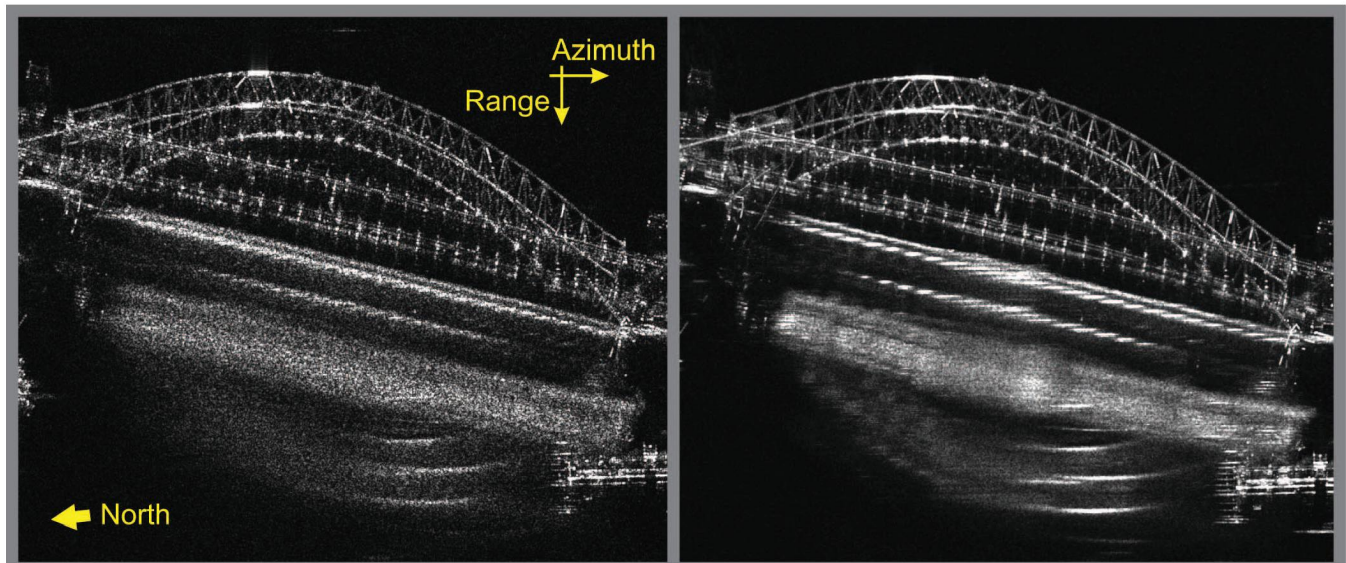
VOLUME 9

NUMBER 3

IJSTHZ

(ISSN 1939-1404)

SPECIAL ISSUE ON SYNTHETIC APERTURE RADAR (SAR)—NEW TECHNIQUES, MISSIONS AND APPLICATIONS



Zoom into TerraSAR-X SAR images of the Sydney Harbour Bridge, Sydney, Australia acquired in high-resolution spotlight mode (left) and in staring spotlight mode (right). Both images are processed to the same resolution of approximately one meter resulting in a higher number of looks for the staring spotlight image (right). The better radiometric resolution of the staring spotlight image facilitates the identification of single scatterers. For more information see “TerraSAR-X Staring Spotlight Mode Optimization and Global Performance Predictions,” by T. Kraus *et al.*, which begins on p. 1015.

IEEE JOURNAL OF SELECTED TOPICS IN APPLIED EARTH OBSERVATIONS AND REMOTE SENSING

A PUBLICATION OF THE IEEE GEOSCIENCE AND REMOTE SENSING SOCIETY
AND THE IEEE COMMITTEE ON EARTH OBSERVATIONS



MARCH 2016

VOLUME 9

NUMBER 3

IJSTHZ

(ISSN 1939-1404)

SPECIAL ISSUE ON SYNTHETIC APERTURE RADAR (SAR)—NEW TECHNIQUES, MISSIONS AND APPLICATIONS

Foreword to the Special Issue on Synthetic Aperture Radar (SAR)—New Techniques, Missions and Applications	G. Krieger, A. Moreira, M. Zink, M. Shimada, and S. Hensley	967
An Airborne Radar Sensor for Maritime and Ground Surveillance and Reconnaissance—Algorithmic Issues and Exemplary Results	M. Kirsch, J. Mietzner, B. Bickert, A. Dallinger, J. Hippler, J. Meyer-Hilberg, R. Zahn, and J. Boukamp	971
Multichannel Wideband Synthetic Aperture Radar for Ice Sheet Remote Sensing: Development and the First Deployment in Antarctica	Z. Wang, S. Gogineni, F. Rodriguez-Morales, J.-B. Yan, J. Paden, C. Leuschen, R. D. Hale, J. Li, C. L. Carabajal, D. Gomez-Garcia, B. Townley, R. Willer, L. Stearns, S. Child, and D. Braaten	980
Independent Verification of the Sentinel-1A System Calibration	M. Schwerdt, K. Schmidt, N. Tous Ramon, G. Castellanos Alfonzo, B. J. Döring, M. Zink, and P. Prats-Iraola	994
WBI Suppression for SAR Using Iterative Adaptive Method	Z. Yang, W. Du, Z. Liu, and G. Liao	1008
TerraSAR-X Staring Spotlight Mode Optimization and Global Performance Predictions	T. Kraus, B. Bräutigam, J. Mittermayer, S. Wollstadt, and C. Grigorov	1015
Synchronization and Processing in the HITCHHIKER Bistatic SAR Experiment	F. Behner, S. Reuter, H. Nies, and O. Loffeld	1028
Enhancing Interferometric SAR Performance Over Sandy Areas: Experience From the TanDEM-X Mission	M. Martone, B. Bräutigam, P. Rizzoli, N. Yague-Martinez, and G. Krieger	1036
The TanDEM-X DEM Mosaicking: Fusion of Multiple Acquisitions Using InSAR Quality Parameters	A. Gruber, B. Wessel, M. Martone, and A. Roth	1047
First Characterization and Performance Evaluation of Bistatic TanDEM-X Experimental Products	J.-L. Bueso-Bello, M. Martone, P. Prats-Iraola, and B. Bräutigam	1058
Analysis of a Maximum Likelihood Phase Estimation Method for Airborne Multibaseline SAR Interferometry	C. Magnard, M. Frioud, D. Small, T. Brehm, and E. Meier	1072
GLRT Based on Support Estimation for Multiple Scatterers Detection in SAR Tomography	A. Budillon and G. Schirinzi	1086
On the Synergistic Use of SAR Constellations' Data Exploitation for Earth Science and Natural Hazard Response	P. Milillo, B. Riel, B. Minchew, S.-H. Yun, M. Simons, and P. Lundgren	1095
A Benchmark Evaluation of Similarity Measures for Multitemporal SAR Image Change Detection	S. Cui, G. Schwarz, and M. Datcu	1101

(Contents Continued on Page 966)



A Modified Frequency Domain Algorithm Based on Optimal Azimuth Quadratic Factor Compensation for Geosynchronous SAR Imaging	Z. Ding, B. Shu, W. Yin, T. Zeng, and T. Long	1119
Motion and Doppler Characteristics Analysis Based on Circular Motion Model in Geosynchronous SAR	T. Zeng, W. Yin, Z. Ding, and T. Long	1132
Background Ionosphere Effects on Geosynchronous SAR Focusing: Theoretical Analysis and Verification Based on the BeiDou Navigation Satellite System (BDS)	C. Hu, Y. Tian, X. Yang, T. Zeng, T. Long, and X. Dong	1143
A Model for the Backscattering From a Canonical Ship in SAR Imagery	P. Iervolino, R. Guida, and P. Whittaker	1163
Polarimetric Simulations of Bistatic Scattering From Perfectly Conducting Ocean Surfaces With 3 m/s Wind Speed at L-Band	J. Yang, Y. Du, and J. Shi	1176
The Dynamic Processes of Sea Ice on the East Coast of Antarctica—A Case Study Based on Spaceborne Synthetic Aperture Radar Data from TerraSAR-X	H. Liu, X.-M. Li, and H. Guo	1187
Late Summer Arctic Sea Ice Surface Roughness Signatures in C-Band SAR Data	A. S. Fors, C. Brekke, S. Gerland, A. P. Doulgeris, and J. F. Beckers	1199
Observations and Simulation of Multifrequency SAR Data Over a Snow-Covered Boreal Forest	F. Montomoli, G. Macelloni, M. Brogioni, J. Lemmetyinen, J. Cohen, and H. Rott	1216
Coupling SAR C-Band and Optical Data for Soil Moisture and Leaf Area Index Retrieval Over Irrigated Grasslands	N. N. Baghdadi, M. El Hajj, M. Zribi, and I. Fayad	1229
A Two-Phase Algorithm Based on Kurtosis Curvelet Energy and Unsupervised Spectral Regression for Segmentation of SAR Images	Z. Tirandaz and G. Akbarizadeh	1244
A Multi-kernel Joint Sparse Graph for SAR Image Segmentation	J. Gu, L. Jiao, S. Yang, F. Liu, B. Hou, and Z. Zhao	1265
Eigen-Decomposition-Based Four-Component Decomposition for PolSAR Data	B. Zou, D. Lu, L. Zhang, and W. M. Moon	1286
A New Image Quality Index for Objectively Evaluating Despeckling Filtering in SAR Images	L. Gomez, M. E. Buemi, J. C. Jacobo-Berlles, and M. E. Mejail	1297
SAR Target Recognition Via Sparse Representation of Monogenic Signal on Grassmann Manifolds	G. Dong and G. Kuang	1308
